Journal Pre-proof

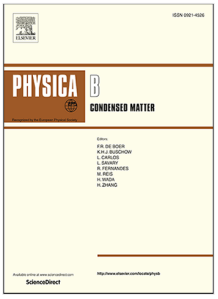

Strain-induced 11.46% solar-to-hydrogen efficiency in Ga_2SO/WTe_2 Z-scheme heterostructure

Mengran Qin, Xiangjie Chen, Jifan Wan, Yao He, Kai Xiong

PII: S0921-4526(25)00770-7
DOI: https://doi.org/10.1016/j.physb.2025.417653
Reference: PHYSB 417653

To appear in: *Physica B: Condensed Matter*

Received date : 18 June 2025
Revised date : 18 July 2025
Accepted date : 29 July 2025

Please cite this article as: M. Qin, X. Chen, J. Wan et al., Strain-induced 11.46% solar-to-hydrogen efficiency in Ga_2SO/WTe_2 Z-scheme heterostructure, *Physica B: Condensed Matter* (2025), doi: https://doi.org/10.1016/j.physb.2025.417653.

This is a PDF file of an article that has undergone enhancements after acceptance, such as the addition of a cover page and metadata, and formatting for readability, but it is not yet the definitive version of record. This version will undergo additional copyediting, typesetting and review before it is published in its final form, but we are providing this version to give early visibility of the article. Please note that, during the production process, errors may be discovered which could affect the content, and all legal disclaimers that apply to the journal pertain.

© 2025 Published by Elsevier B.V.

Journal Pre-proof

Highlights

Strain-Induced 11.46% Solar-to-Hydrogen Efficiency in Ga_2SO/WTe_2 Z-scheme Heterostructure

Mengran Qin, Xiangjie Chen, Jifan Wan, Yao He, Kai Xiong

- Strain-induced solar-to-hydrogen efficiency of **11.46%** (10.55% with field corrections) in Ga_2SO/WTe_2 heterostructure, surpassing most reported Z-scheme photocatalysts.
- Direct Z-scheme charge transfer confirmed by differential charge density and Bader analysis, with built-in electric field enabling efficient carrier separation.
- Broad-spectrum absorption (UV to visible) and strain-tunable band alignment overcoming the 1.23 eV thermodynamic limit for water splitting.

Journal Pre-proof

Journal Pre-proof

Strain-Induced 11.46% Solar-to-Hydrogen Efficiency in Ga_2SO/WTe_2 Z-scheme Heterostructure

Mengran Qin[a], Xiangjie Chen[a], Jifan Wan[a], Yao He[a,*] and Kai Xiong[b]

[a]Department of Physics, Yunnan University, , Kunming, 650091, China
[b]Materials Genome Institute, Yunnan University, Kunming, 650091, China

ARTICLE INFO

Keywords:
Van der Waals heterostructure
Direct Z-scheme photocatalyst
Strain-tunable
Solar-to-hydrogen efficiency
Photocatalytic water-splitting

ABSTRACT

We propose a novel Ga_2SO/WTe_2 van der Waals heterostructure as a direct Z-scheme photocatalyst, confirmed through differential charge density calculations and Bader charge analysis. The system exhibits strain-tunable solar-to-hydrogen efficiency, with biaxial strain (-8% to +8%) effectively modulating its electronic properties and achieving maximum η_{STH} and η'_{STH} values of 11.46% and 10.55%, respectively. The Ga_2SO/WTe_2 heterostructure exhibits a staggered band alignment while demonstrating strong optical absorption across visible to ultraviolet wavelengths. Furthermore, the constituent monolayers show significant exciton binding energies of 1.12 eV (Ga_2SO) and 0.54 eV (WTe_2). Although our Gibbs free energy calculations reveal that the Ga_2SO/WTe_2 heterostructure exhibits non-spontaneous oxygen evolution reaction (OER) and hydrogen evolution reaction (HER) thermodynamics, comparative studies highlight its promising catalytic functionality. This work provides a promising route for designing high-efficiency photocatalytic water-splitting catalysts with tunable electronic and optical properties.

1. Introduction

The current reliance on conventional energy sources (e.g., petroleum and fossil fuels) faces growing challenges due to their non-renewable nature and associated greenhouse gas emissions.[1, 2] Photocatalytic water splitting has emerged as a promising alternative since Fujishima and Honda's pioneering demonstration of TiO_2 photocatalysis in 1972.[3] Semiconductor photocatalysts now attract significant attention for solar-driven water splitting and pollutant degradation.[4, 5] An ideal photocatalyst must simultaneously satisfy four critical requirements: (i) an appropriate bandgap for broad solar spectrum absorption, (ii) staggered band alignment for efficient charge separation, (iii) sufficient redox potentials to drive both hydrogen and oxygen evolution reactions (HER/OER), and (iv) excellent operational stability.[6, 7] Two-dimensional (2D) materials have shown particular promise in this regard.[8, 9, 10, 11] However, most single-component 2D materials fail to meet all these criteria simultaneously.

Heterostructure engineering has proven to be an effective strategy to overcome these limitations. By carefully designing van der Waals heterostructures, researchers can precisely tune electronic properties, optimize band edge alignment, and ultimately enhance photocatalytic efficiency.[12, 13, 14] This approach not only addresses the inherent drawbacks of individual 2D materials but also enables the development of next-generation photocatalysts with superior performance. In the construction of heterostructures for photocatalytic water splitting, two predominant band alignment configurations emerge: the Type-II band structure and Z-scheme heterostructures.[15, 16] The fundamental distinction between Type-II and Z-scheme heterostructures lies in their interfacial charge transfer mechanisms driven by layer coupling effects, leading to divergent built-in electric field directions. In Type-II heterostructures, the built-in field causes photogenerated electrons and holes to accumulate at the conduction band minimum (CBM) and valence band maximum (VBM) of different layers, respectively, participating in redox reactions with weakened potential. Distinct from the Type-II arrangement, Z-scheme systems exhibit an inverted built-in electric field orientation, which drives the recombination of photogenerated carriers between the CBM of one constituent material and the VBM of the other. This charge transfer mechanism effectively segregates the HER to the component with higher CBM potential while localizing the OER at the component with lower VBM potential. [17]Crucially, this architecture preserves the intrinsic redox capabilities of both constituents, thereby overcoming the fundamental 1.23 eV thermodynamic requirement for water splitting.[18, 19, 20] The Z-scheme approach not only enhances photocatalytic efficiency but also significantly expands the range of viable materials for solar energy conversion applications.

By selectively replacing X atoms with oxygen (O) on one side of GaX monolayers, Demirtas *et al.* designed a novel two-dimensional ternary Ga_2XO structure (X = S, Se, Te) through controlled oxidation, demonstrating significant modifications to the electronic structure.[21] The resulting Janus Ga_2XO monolayer exhibits enhanced charge carrier separation efficiency due to its intrinsic asymmetric structure that generates a spontaneous built-in electric field.[22] This symmetry-breaking effect in the 2D material effectively suppresses electron-hole recombination, thereby enhancing

*Corresponding author
email=yhe@ynu.edu.cn (Y. He)
ORCID(s):

Journal Pre-proof

photocatalytic performance. Recent advances have highlighted two-dimensional transition metal dichalcogenides (2D TMDs) as ideal building blocks for van der Waals heterostructures,[23, 24, 25] enabling both fundamental studies of novel physical phenomena and practical device applications. Among these, tungsten ditelluride (WTe_2) has emerged as particularly promising, with monolayer samples successfully synthesized via various methods including chemical vapor deposition (CVD)[26, 27] and molecular beam epitaxy (MBE)[28]. Notably, the GaS/WTe_2 van der Waals heterostructure reported by Wan *et al.* demonstrates exceptional photocatalytic water-splitting performance as a direct Z-scheme photocatalyst.[29] Theoretical work by Yang *et al.* systematically investigated the structural, optoelectronic, and photocatalytic properties of g-C_6N_6/WTe_2 heterostructures using first-principles calculations, confirming their Z-scheme characteristics.[30]

In this work, we systematically constructed six distinct configurations of van der Waals Ga_2SO/WTe_2 heterostructures through vertical stacking of monolayer WTe_2 and Ga_2SO. *Ab initio* molecular dynamics simulations (AIMD) and phonon calculations confirmed the structural stability of four out of the six investigated configurations. Comprehensive hybrid functional calculations of band structures and charge distribution analysis revealed the formation of a direct Z-scheme photocatalytic system in the optimized Ga_2SO/WTe_2 heterostructures. Through biaxial strain modulation (-8% to +8%), we achieved tunable conversion efficiency from solar to hydrogen (STH) up to 11.46% (10.55% with field corrections), demonstrating strain engineering as an effective approach for optimizing photocatalytic performance in Ga_2SO/WTe_2 heterostructures. Optical calculations demonstrated that while the Ga_2SO monolayer primarily absorbs in the ultraviolet region, the Ga_2SO/WTe_2 heterostructure exhibits significantly broadened absorption extending well into the visible spectrum. Thermodynamic analysis of Gibbs free energy changes further verifid the feasibility for both HER and OER. These results collectively establish the Ga_2SO/WTe_2 heterostructure as a strain-tunable Z-scheme photocatalyst with broad-spectrum absorption and efficient redox functionality.

2. Computational Details

First principles calculations were performed using VASP 6.3.3[31] with PAW pseudopotentials[32]. Structural relaxations employed PBE-GGA[33], while optical absorption coefficients were calculated with HSE06[34], and exciton binding energies were obtained via G_0W_0+BSE[35, 36] (400/200 eV cutoffs for wavefunctions/response functions). The DFT-D3 method[37] accounted for vdW interactions, with a 520 eV plane-wave cutoff, $8\times8\times1$ Γ-centered k-mesh, and convergence criteria of 10^{-6} eV and 0.005 eV/ Å. A > 15 Å vacuum layer was included. Thermodynamic stability was confirmed by AIMD[38, 39] (300 K, 10 ps, $3\times3\times1$ supercell), and phonon spectra were computed via the finite-displacement method[40, 41].

3. Results and Discussion

3.1. Geometrical structures and stability of Ga_2SO/WTe_2 heterostructure

Before investigating the Ga_2SO/WTe_2 heterostructure, we first geometrically optimized the isolated Ga_2SO and 2H-phase WTe_2 monolayers, as shown in Fig. S1 (a) and (c), respectively. The optimized lattice constants are 3.36 Å for Ga_2SO and 3.51 Å for WTe_2, with both monolayers belonging to the P3m1 space group. We employed HSE06 calculations to determine accurate band gap values. As presented in Fig. S1 (b) and (d), both Ga_2SO and WTe_2 monolayers exhibit direct bandgaps of 2.09 eV and 1.60 eV, respectively. The VBM and CBM are located at the Γ point for Ga_2SO and at point K for WTe_2. These calculated lattice constants and bandgaps agree well with previous reports,[42, 43, 44, 45] validating our computational methodology. The work functions were calculated from the energy difference between the vacuum level and Fermi level, with the electrostatic potential shown in Fig. S2. The WTe_2 monolayer shows a work function of 4.88 eV. For Ga_2SO, symmetry breaking creates a 0.51 eV vacuum level difference between surfaces, resulting in work functions of 6.08 eV and 6.59 eV for the two surfaces, respectively.

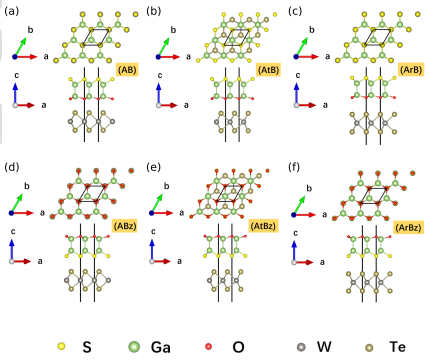

Figure 1: Top and side views of the Ga_2SO/WTe_2 heterostructure. The black rectangle represents the primitive cell used in our calculations.

The lattice mismatch rate of the Ga_2SO/WTe_2 heterostructure was calculated according to the following formula, with a determined value of 4.37%.

$$\delta = 2\times\frac{|a_1 - a_2|}{a_1 + a_2}$$

where a_1 and a_2 represent the lattice constants of the pristine Ga_2SO and WTe_2 monolayers, respectively. Based on the symmetry of the lattice, we constructed six stacking configurations for the Ga_2SO/WTe_2 heterostructure, which are designated as AB, AtB, ArB, ABz, AtBz and ArBz, as illustrated in Fig. 1. The formation energy E_F for the six heterostructure configurations was calculated using the

Journal Pre-proof

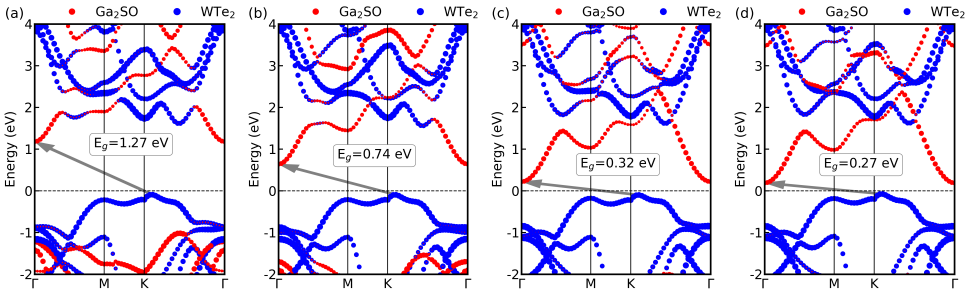

Figure 2: Projected band structures of Ga_2SO/WTe_2 heterostructures for different configurations: (a) AB, (b) AtB, (c) ABz, and (d) AtBz.

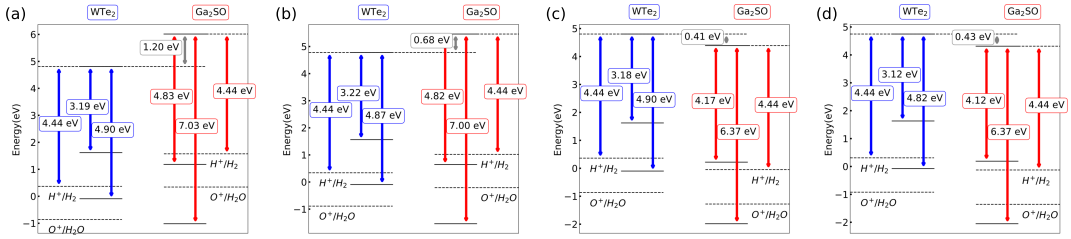

Figure 3: Comparison of band alignment and photocatalytic water splitting energy levels (PH=0) at the vacuum level in the Ga_2SO/WTe_2 heterostructures: (a) AB, (b) AtB, (c) ABz, and (d) AtBz.

following formula:

$$E_{\mathrm{F}} = E_{\mathrm{Ga_2SO/WTe_2}} - E_{\mathrm{Ga_2SO}} - E_{\mathrm{WTe_2}}$$

where E_{Ga_2SO/WTe_2}, E_{Ga_2SO} and E_{WTe_2} represent the energy of the Ga_2SO/WTe_2 heterostructures, the Ga_2SO monolayer and the WTe_2 monolayer, respectively. The negative value of the formation energy signifies structural stability, where more negative values correspond to higher stability. The optimized lattice constants, interlayer distances and the formation energy of the Ga_2SO/WTe_2 heterostructure are summarized in Table S1. We can observe that the six heterostructure configurations exhibit lattice constants of approximately 3.44 Å, interlayer distance ranging from 2.95 to 3.82 Å, and formation energies between −110.81 eV and −206.56 eV. Notably, the AB configuration demonstrates the smallest interlayer distance and the most negative formation energy, indicating that it is the most stable among the six configurations.

The phonon spectra were calculated for the six configurations of the Ga_2SO/WTe_2 heterostructure, as illustrated in Fig. S3. AIMD simulations under the canonical NVT ensemble adopted with a Nosé thermostat[38] was performed, as shown in Fig. S4. The Ga_2SO/WTe_2 heterostructures of configurations ArB and ArBz exhibit noticeable imaginary frequencies in their phonon spectra at the Γ point, indicating structural instabilities. Furthermore, AIMD calculations reveal structural distortions of configurations ArB and ArBz during simulations, accompanied by energy fluctuations that deviate significantly from a stable average value. These results collectively demonstrate that the Ga_2SO/WTe_2 heterostructures of configurations ArB and ArBz are unstable. However, the other four Ga_2SO/WTe_2 heterostructures configurations demonstrate both dynamic and thermodynamic stability. Their phonon spectra show no significant soft modes or imaginary frequencies throughout the entire Brillouin zone, except for a negligible imaginary frequency at the Γ point. Moreover, AIMD simulations reveal that these configurations maintain structural integrity with no bond breaking, while the system energy fluctuates consistently around an equilibrium value. Therefore, we will subsequently focus on investigating the electronic and optical properties of Ga_2SO/WTe_2 heterostructures with configurations AB, AtB, ABz and AtBz. The mechanical stability of the Ga_2SO/WTe_2 heterostructures was further verified based on the calculation of elastic constants using Born-Huang's criterion[46]. For the hexagonal crystal structure of the Ga_2SO/WTe_2 heterostructures, only two independent elastic constants, C_{11} and C_{12}, need to be calculated, while C_{66} can be derived as

$$C_{66} = \frac{C_{11} - C_{12}}{2}.$$

Journal Pre-proof

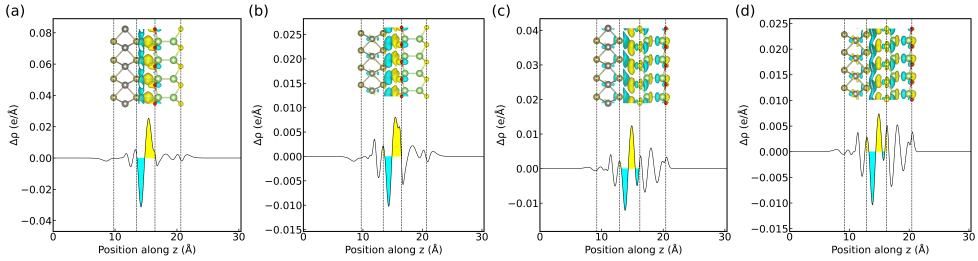

Figure 4: Plane-averaged differential charge density of the Ga_2SO/WTe_2 heterostructure for (a) AB, (b) AtB, (c) ABz, and (d) AtBz configurations. Full lines mark the edge positions of the two monolayers. The yellow and cyan represent charge accumulation and depletion, respectively.

The calculated values for the four configurations are presented in Table S2 of the Supplementary Material. These values satisfy the mechanical stability criteria $C_{11} > 0$ and $C_{11} > C_{12}$, confirming the mechanical stability of the Ga_2SO/WTe_2 heterostructure.

3.2. Electronic properties and built-in electric field in Ga_2SO/WTe_2 heterostructure

The band structures of the four stacking configurations of the Ga_2SO/WTe_2 heterostructure, calculated using the HSE06 functional, are shown in Fig. 2. The energy bands of the four types of the Ga_2SO/WTe_2 heterostructures all exhibit indirect band gaps. The band gap values for AB, AtB, ABz, and AtBz are 1.27, 0.74, 0.32, and 0.27 eV, respectively. In the projected band structure depicted in Fig. 2, the red dots signify contributions from the Ga_2SO monolayer, while the blue dots denote contributions from the WTe_2 monolayer. It is evident that across all four configurations of the Ga_2SO/WTe_2 heterostructures, the CBM is predominantly contributed by the Ga_2SO monolayer, and the VBM is primarily contributed by the WTe_2 monolayer. The staggered band alignment is conducive to the transfer of photogenerated electrons, facilitating their movement across the interface and potentially enhancing the efficiency of charge separation in photocatalytic applications.

The electrostatic potential for the four configurations (Fig. S5) reveal a vacuum level difference between the constituent monolayers in the heterostructures. As shown in Fig. 3, the band edge positions of the Ga_2SO/WTe_2 heterostructures do not straddle the redox potentials for photocatalytic water splitting in any of the four configurations. These results indicate that none of these configurations of the Ga_2SO/WTe_2 heterostructure meet the conventional electronic structure requirements for traditional photocatalytic water decomposition.

The direction of the built-in electric fields in the interlayers of the Ga_2SO/WTe_2 heterostructures is determined by the differential charge density (Δ_ρ) and further confirmed by Bader charge analysis. The formula for calculating the planar average differential charge density is as follows:

$$\Delta_\rho = \rho_{Ga_2SO/WTe_2} - \rho_{Ga_2SO} - \rho_{WTe_2}$$

where ρ_{Ga_2SO/WTe_2}, ρ_{Ga_2SO} and ρ_{WTe_2} are the charge density of the Ga_2SO/WTe_2 heterostructures, the Ga_2SO monolayer, and the WTe_2 monolayer, respectively. The results are shown in Fig. 4. It is evident that charge accumulation occurs in the Ga_2SO monolayers, whereas charge depletion is observed in the WTe_2 monolayers. Furthermore, the Bader charge analysis reveals that a charge transfer of 0.031, 0.020, 0.018 and 0.017 $|e|$ occurs from the WTe_2 monolayers to the Ga_2SO monolayer in the AB, AtB, ABz and AtBz configurations, respectively. The minimal interlayer charge transfer values suggest that the interaction between the layers is relatively weak. The higher work function of the Ga_2SO monolayer compared to the WTe_2 monolayer aligns with the observed direction of charge transfer, suggesting that the electronic potential difference drives the charge redistribution between the two monolayers. In conclusion, the built-in electric field in the Ga_2SO/WTe_2 heterostructures is directed from WTe_2 to Ga_2SO. This field drives the spatial separation of photogenerated carriers, confining holes in Ga_2SO and electrons in WTe_2 while enabling their redox-capable counterparts to recombine. The resulting charge separation preserves strong redox capabilities and suppresses recombination, forming an efficient Z-scheme system.[47, 48]

3.3. Optical absorption, STH and strain engineering control

In the Ga_2SO/WTe_2 heterostructure, the hydrogen evolution reaction and oxygen evolution reaction take place on the WTe_2 monolayer and the Ga_2SO monolayer, respectively. To understand their individual contributions, we computed the optical absorption coefficients of the two isolated monolayers extracted from the Ga_2SO/WTe_2 heterostructure using HSE06 method are presented in Fig. 5. The optical absorption coefficient is given:

$$\alpha(\omega) = \sqrt{2}\omega\sqrt{\sqrt{\varepsilon_1^2(\omega) + \varepsilon_2^2(\omega)} - \varepsilon_1(\omega)}$$

where ω is the angular frequency, and $\varepsilon_1(\omega)$ and $\varepsilon_2(\omega)$ are the real and imaginary parts of the dielectric function, respectively.[49] It can be observed that the separated WTe_2 monolayer exhibits significant optical absorption across both the visible and ultraviolet spectral regions. In contrast, the

Journal Pre-proof

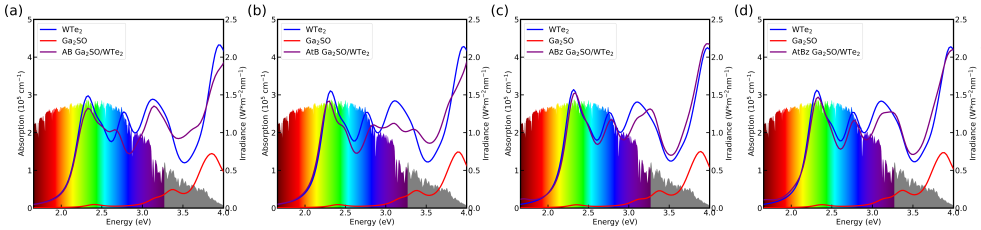

Figure 5: Absorption coefficients for the Ga_2SO/WTe_2 heterostructures and isolated monolayers extracted from the heterostructure of four configurations.

isolated Ga_2SO monolayer demonstrates relatively weaker absorption in the visible range, with its primary absorption peak occurring predominantly in the ultraviolet region. Furthermore, it can be observed that the Ga_2SO/WTe_2 heterostructures exhibits excellent light absorption capabilities in both the visible and ultraviolet spectral regions. This is consistent with previous reports where the optical absorption coefficient of heterostructures are generally enhanced compared to their constituent monolayers.[50]

Additionally, the single-shot G_0W_0+BSE method was employed to determine the quasi-particle band gaps and optical gaps of pristine WTe_2 and Ga_2SO monolayers. Our calculations reveal that the quasi-particle band gaps for the Ga_2SO and WTe_2 monolayers are 3.00 eV and 2.11 eV, respectively, while the corresponding optical gaps are 1.88 eV and 1.57 eV. The exciton binding energies, obtained from the difference between the quasi-particle band gaps and optical gaps, are found to be 1.12 eV for Ga_2SO and 0.54 eV for WTe_2. The larger quasi-particle bandgap of Ga_2SO monolayer yields a higher exciton binding energy (E_b) than WTe_2 monolayer. Although elevated E_b promotes exciton accumulation, it concurrently intensifies excitonic effects-strengthening Coulomb interactions that may hinder charge separation and thus limit photocatalytic efficiency.[49, 51] The corresponding oscillator strengths are presented in Fig. S6.

The photocatalytic performance of the constructed Z-scheme Ga_2SO/WTe_2 heterostructures was quantitatively evaluated using the conversion efficiency from solar to hydrogen (η_{STH}), as proposed by Fu et al.[52, 53]. This metric provides a comprehensive assessment of the system's ability to harness solar energy for hydrogen production, taking into account factors such as light absorption, charge carrier separation, and surface redox reactions. The higher the η_{STH} value, the more efficient the photocatalytic system is in converting solar energy into chemical energy, which is critical for practical applications in renewable energy. The built-in electric field in the Ga_2SO/WTe_2 heterostructures induces work function differences that significantly influence the photocatalytic water splitting process. To eliminate potential biases, the corrected solar-to-hydrogen efficiency (η'_{STH}) was additionally calculated. We applied strains ranging from -8% to 8% to the structure and calculated changes in the band structure and corrected solar-to-hydrogen efficiency of the Ga_2SO/WTe_2 heterostructure under strain, as shown in Fig. 6 and Table S3-S6. The results reveal that the band structure, η_{STH} and η'_{STH} of the Ga_2SO/WTe_2 heterostructure exhibit significant variations under different strain conditions. Among all strain conditions, the AtB configuration exhibits the highest solar-to-hydrogen efficiencies, with η_{STH} and η'_{STH} reaching 11.46% and 10.55% under 8% tensile strain, respectively. The strain-tunable electronic properties of the Ga_2SO/WTe_2 heterostructure, combined with its high solar-to-hydrogen conversion efficiency, make it a promising candidate for practical photocatalytic applications.

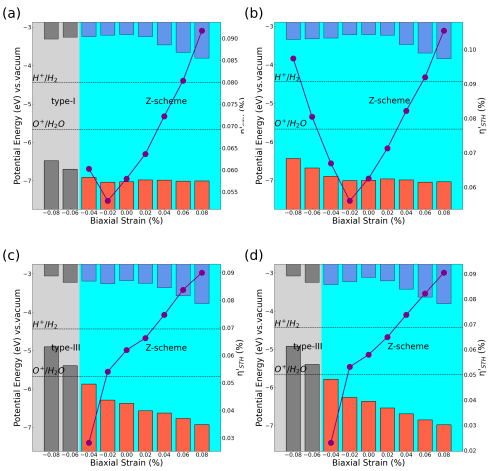

Figure 6: The band edges and corrected solar-to-hydrogen conversion efficiencies (PH=0) for the AB, AtB, ABz, and AtBz configurations of the Ga_2SO/WTe_2 heterostructures under biaxial strains ranging from −8% to 8%. The red and blue columns represent the VBM of the Ga_2SO monolayer and the CBM of the WTe_2 monolayer, respectively. The grey columns indicate cases where the band edges fail to satisfy the potential requirements for photocatalytic water splitting.

Journal Pre-proof

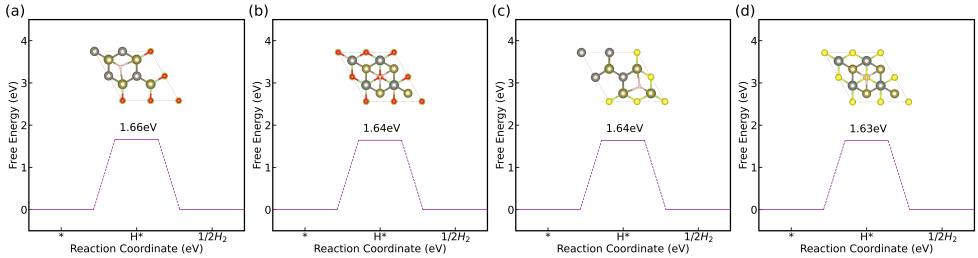

Figure 7: Gibbs free energy changes for the hydrogen evolution reaction on the WTe_2 monolayer in four Ga_2SO/WTe_2 heterostructures configurations: (a) AB, (b) AtB, (c) ABz, (d) AtBz.

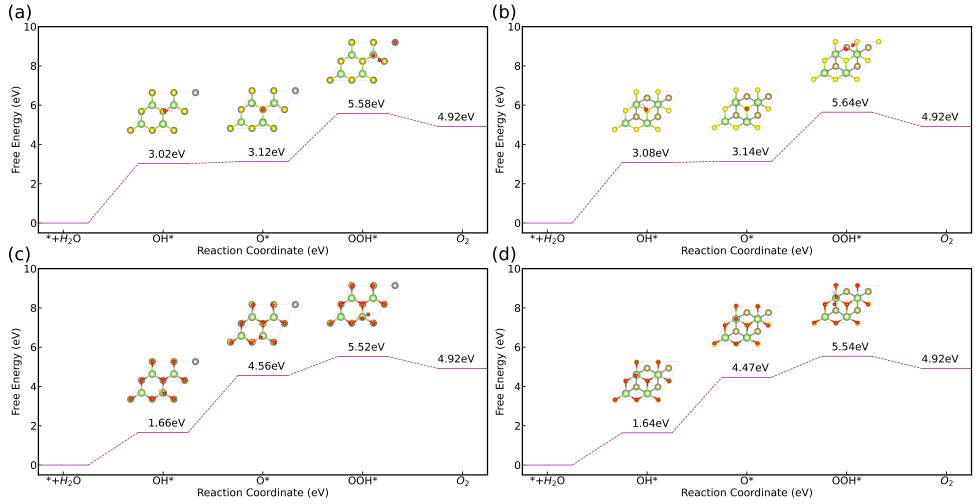

Figure 8: Gibbs free energy changes for the oxygen evolution reaction on the Ga_2SO monolayer in four Ga_2SO/WTe_2 heterostructures configurations: (a) AB, (b) AtB, (c) ABz, (d) AtBz.

3.4. Gibbs free energies and thermodynamics feasibility

The Gibbs free energy profiles for both the hydrogen evolution reaction on WTe_2 surfaces and the oxygen evolution reaction on Ga_2SO surfaces were systematically evaluated using density functional theory, as detailed in the Supplementary Materials. This analysis elucidates the thermodynamic feasibility of these reactions driven by the Ga_2SO/WTe_2 heterostructure as shown in Fig. 7 and Fig. 8. The Gibbs free energy for the hydrogen evolution reaction across the four Ga_2SO/WTe_2 heterostructure configurations ranges from 1.63 eV to 1.66 eV. In contrast, the band alignment analysis reveals a photogenerated bias of only 1.22-1.32 eV for HER. This significant discrepancy suggests that the HER process in these Ga_2SO/WTe_2 heterostructures cannot proceed spontaneously under the given conditions, as the thermodynamic driving force provided by the photoexcitation is insufficient to overcome the reaction energy barrier. Notably, the Gibbs free energy for the hydrogen evolution reaction in this work (1.63-1.66 eV) is lower than the experimentally reported values for N-doped Ni_3S_2 (2.7 eV)[54] and graphene/MoS_2 heterostructures (2.01 eV)[55]. This comparison suggests that the HER activity of Ga_2SO/WTe_2 heterostructures may be experimentally achievable, although additional catalytic enhancement might be required to overcome the remaining energy barrier.

The oxygen evolution reaction at the monolayer Janus Ga_2SO interface exhibits configuration-dependent energetics: The AB and AtB configurations show OH* formation as the rate-determining step (RDS) with ΔG_{RDS} of 3.02 eV and 3.08 eV, respectively, while the ABz and AtBz configurations shift the RDS to O* formation with ΔG_{RDS} = 2.90 eV and 2.83 eV, respectively. This transition originates from the symmetry breaking in the Janus Ga_2SO monolayer, which modifies the local adsorption configuration. Although the photogenerated bias for OER in pristine Ga_2SO/WTe_2 heterostructures (1.93–2.59 eV) is insufficient to drive spontaneous oxygen evolution, established doping

Journal Pre-proof

strategies have been proven effective in reducing the thermodynamic overpotential for analogous 2D materials [56, 57]. This precedent supports the experimental feasibility of OER in Ga_2SO/WTe_2 systems upon appropriate structural modifications, though detailed engineering approaches require further investigation.

4. Conclusion

This study presents the design and characterization of the Ga_2SO/WTe_2 van der Waals heterostructure through first-principles calculations, with systematic investigation of its photocatalytic water-splitting properties. Combined differential charge density and Bader charge analyses reveal an interfacial built-in electric field that establishes a direct Z-scheme charge transfer pathway, enabling both efficient carrier separation and preservation of high-redox-capacity charges. Through systematic strain engineering, the heterostructure achieves maximum solar-to-hydrogen efficiencies of 11.46% (η_{STH}) and 10.55% (η'_{STH}) under optimal biaxial strain conditions, representing superior performance among contemporary photocatalyst systems. Detailed optical calculations reveal that the WTe_2 monolayer exhibits strong absorption across both visible and ultraviolet regions, while the Ga_2SO monolayer shows prominent absorption only in the ultraviolet region. Remarkably, the constructed heterostructure maintains enhanced light absorption spanning the entire visible-to-UV spectrum, which correlates well with its excellent photocatalytic performance. Gibbs free energy calculations reveal thermodynamic limitations for OER/HER in the pristine Ga_2SO/WTe_2 heterostructure. However, comparative studies suggest that such energy barriers could potentially be reduced through material engineering approaches, as evidenced in other 2D catalytic systems, making experimental realization feasible. These computational results suggest that the Ga_2SO/WTe_2 heterostructure represents a promising candidate for photocatalytic water-splitting applications, and further experimental validation would be valuable.

Conflicts of interest

There are no conflicts to declare.

Acknowledgements

This work was supported by the National Natural Science Foundation of China (Grant Nos. 12164050 and 12264022), the Major Science and Technology Project of Precious Metal Materials Genetic Engineering in Yunnan Province (Grant Nos. 2019ZE001-1, 202002AB080001-6, and 2018IC058), the Program for Yunling Scholars in Yunnan Province and the Program for Donglu Scholars in Yunnan University.

References

[1] David Dodman. Forces driving urban greenhouse gas emissions. *Current Opinion in Environmental Sustainability*, 3(3):121–125, 2011.

[2] Hsiao-Tien Pao and Chung-Ming Tsai. CO_2 emissions, energy consumption and economic growth in BRIC countries. *Energy Policy*, 38(12):7850–7860, 2010.

[3] A. Fujishima and K. Honda. Electrochemical photolysis of water at a semiconductor electrode. *Nature*, 238(5358):37–38, 1972.

[4] T. Jafari, E. Moharreri, A. Amin, R. Miao, W. Song, and S. Suib. Photocatalytic water splitting—The untamed dream: A review of recent advances. *Molecules*, 21(7):900, 2016.

[5] Gian Luca Chiarello, Myriam H. Aguirre, and Elena Selli. Hydrogen production by photocatalytic steam reforming of methanol on noble metal-modified TiO_2. *Journal of Catalysis*, 273(2):182–190, 2010.

[6] Irshad Ahmad, Yanhong Zou, Jiaying Yan, Yuyu Liu, Shazia Shukrullah, Muhammad Yasin Naz, Humaira Hussain, Waheed Qamar Khan, and N.R. Khalid. Semiconductor photocatalysts: A critical review highlighting the various strategies to boost the photocatalytic performances for diverse applications. *Advances in Colloid and Interface Science*, 311:102830, 2023.

[7] Cen-Feng Fu, Qiquan Luo, Xingxing Li, and Jinlong Yang. Two-dimensional van der waals nanocomposites as Z-scheme type photocatalysts for hydrogen production from overall water splitting. *J. Mater. Chem. A*, 4:18892–18898, 2016.

[8] Di Gu, Xiaoma Tao, Hongmei Chen, Weiling Zhu, Yifang Ouyang, and Qing Peng. Enhanced photocatalytic activity for water splitting of blue-phase GeS and GeSe monolayers via biaxial straining. *Nanoscale*, 11:2335–2342, 2019.

[9] Tong Chen, Lizhen Liu, Cheng Hu, and Hongwei Huang. Recent advances on Bi_2WO_6-based photocatalysts for environmental and energy applications. *Chinese Journal of Catalysis*, 42(9):1413–1438, 2021.

[10] Yijing Ren, Xinguo Ma, Gang Yuan, Jiajun Liao, Nan Ma, Di Li, and Hui Lv. Two-dimensional tetragonal AlOX (X = Cl, Br, or I) monolayers with promising photocatalytic performance: first-principles investigations. *Phys. Chem. Chem. Phys.*, 26:16765–16773, 2024.

[11] Fengxian Ma, Xiaoxia Liu, Zhen Gao, Zibo Chen, Yalong Jiao, and Zhongfang Chen. Unveiling the photocatalytic potential of two-dimensional ferroelastic LuSX monolayers for efficient water splitting: a first-principles discovery. *J. Mater. Chem. A*, 13:5909–5918, 2025.

[12] Qi-Kang Yin, Chuan-Lu Yang, Mei-Shan Wang, and Xiao-Guang Ma. Two-dimensional heterostructures of AuSe/SnS for the photocatalytic hydrogen evolution reaction with a Z-scheme. *J. Mater. Chem. C*, 9:12231–12238, 2021.

[13] Lin Ju, Ying Dai, Wei Wei, Mengmeng Li, and Baibiao Huang. Dft investigation on two-dimensional GeS/WS_2 van der waals heterostructure for direct Z-scheme photocatalytic overall water splitting. *Applied Surface Science*, 434:365–374, 2018.

[14] X. F. Chen, W. N. Han, Z. Z. Tian, Q. Yue, C. X. Peng, C. Wang, B. Wang, H. B. Yin, and Q. F. Gu. Exploration of photocatalytic overall water splitting mechanisms in the Z-scheme SnS_2/β-As heterostructure. *J. Phys. Chem. C*, 127:6347–6355, 2023.

[15] The-Hung Mai, Rohit Kumar, Vatika Soni, Pardeep Singh, Tahir Iqbal, Alagarsamy S.K. Kumar, Van-Huy Nguyen, Pankaj Raizada, and Phuong V. Pham. 2D heterostructures in photocatalysis for emerging applications: Current status, challenges, and prospectives. *Journal of Catalysis*, 439:115744, 2024.

[16] Jun Liu, Nanke Ma, Wei Wu, and Quanguo He. Recent progress on photocatalytic heterostructures with full solar spectral responses. *Chemical Engineering Journal*, 393:124719, 2020.

[17] Mei-Ling Xu, Meng Lu, Guan-Ying Qin, Xiu-Mei Wu, Ting Yu, Li-Na Zhang, Kui Li, Xin Cheng, and Ya-Qian Lan. Piezo-photocatalytic synergy in $BiFeO_3$/COF Z-scheme heterostructures for high-efficiency overall water splitting. *Angewandte Chemie International Edition*, 61(44):e202210700, 2022.

[18] Wang Y. Dong CL. et al. Zhao, D. Boron-doped nitrogen-deficient carbon nitride-based Z-scheme heterostructures for photocatalytic overall water splitting. 6:388–397, 2021.

[19] Praveen Kumar Basivi, Yogapriya Selvaraj, Sakthivel Perumal, Arjun Kumar Bojarajan, Xianzhong Lin, Maheshwaran Girirajan,

Journal Pre-proof

Chang Woo Kim, and Sambasivam Sangaraju. Graphitic carbon nitride ($g–C_3N_4$)–based Z-scheme photocatalysts: Innovations for energy and environmental applications. *Materials Today Sustainability*, 29:101069, 2025.

[20] Yufei Xue, Lei Gao, Qingyan Li, Wuyi Gao, Jianchen Lu, and Jinming Cai. Z-scheme group-11-chalcogenides heterostructures for solar-driven photocatalytic water splitting. *International Journal of Hydrogen Energy*, 93:992–999, 2024.

[21] M. Demirtas, B. Ozdemir, Y. Mogulkoc, and E. Durgun. Oxygenation of monolayer gallium monochalcogenides: Design of two-dimensional ternary Ga_2XO(X=S, Se, Te). *Phys. Rev. B*, 101:075423, Feb 2020.

[22] Hoi D. Bui, Hamad Rahman Jappor, and Nguyen N. Hieu. Tunable optical and electronic properties of Janus monolayers Ga_2SSe, Ga_2STe, and Ga_2SeTe as promising candidates for ultraviolet photodetectors applications. *Superlattices and Microstructures*, 125:1–7, 2019.

[23] Xiangwei Lu, Yiying Lu, Congjian Wang, and Yang Cao. Efficient photoelectrodes based on two-dimensional transition metal dichalcogenides heterostructures: from design to construction. *Rare Metals*, 41:1142 – 1159, 2022.

[24] Yang X. Liu Y. Li, J. et al. General synthesis of two-dimensional van der waals heterostructure arrays. *Nature*, 579:368–374, 2020.

[25] Lixin Liu and Tianyou Zhai. Wafer-scale vertical van der waals heterostructures. *InfoMat*, 3(1):3–21, 2021.

[26] Jie Li, Shuai Cheng, Zhixuan Liu, Wenfeng Zhang, and Haixin Chang. Centimeter-Scale, Large-Area, Few-Layer 1T'-WTe_2 Films by Chemical Vapor Deposition and Its Long-Term Stability in Ambient Condition. *The Journal of Physical Chemistry C*, 122(12):7005–7012, 2018.

[27] Ilhan C. Balsamo B. Mc Manus, J.B. et al. Synthesis of tungsten ditelluride thin films and highly crystalline nanobelts from pre-deposited reactants. *Tungsten*, 2:321–334, 2020.

[28] Qingxiao Wang Adam T Barton Rafik Addou Christopher M Smyth Hui Zhu Jiyoung Kim Luigi Colombo Moon J Kim Lee A Walsh, Ruoyu Yue. WTe_2 thin films grown by beam-interrupted molecular beam epitaxy. *IOP Publishing*, 4(2):025044, 2017.

[29] Changxin Wan, Wei Yan, Chunsheng Liu, Lan Meng, and Xiaohong Yan. First-principles study of direct Z-scheme GaS/WTe_2 van der waals heterostructure as photocatalyst for water splitting. *Physica B: Condensed Matter*, 682:415882, 2024.

[30] Jian Yang, Xiumei Wei, Zhenduo Wang, Yuhong Huang, Gangqiang Zhu, Shuang Han, and Jianmin Zhang. The direct Z-scheme g-C_6N_6/WTe_2 van der Waals heterojunction as photocatalyst over water splitting in the visible light: Designing strategy from first principles. *Journal of Photochemistry and Photobiology A: Chemistry*, 435:114263, 2023.

[31] G. Kresse and J. Furthmüller. Efficiency of ab-initio total energy calculations for metals and semiconductors using a plane-wave basis set. *Computational Materials Science*, 6(1):15–50, 1996.

[32] P.E. Blöchl. Projector augmented-wave method. *Physical Review B*, 50(24):17953 – 17979, 1994.

[33] John P. Perdew, Kieron Burke, and Matthias Ernzerhof. Generalized gradient approximation made simple. *Phys. Rev. Lett.*, 77:3865–3868, Oct 1996.

[34] Jochen Heyd, Gustavo E. Scuseria, and Matthias Ernzerhof. Hybrid functionals based on a screened coulomb potential. *Journal of Chemical Physics*, 118(18):8207 – 8215, 2003.

[35] M. Shishkin and G. Kresse. Implementation and performance of the frequency-dependent GW method within the paw framework. *Phys. Rev. B*, 74:035101, Jul 2006.

[36] Michael Rohlfing and Steven G. Louie. Electron-hole excitations and optical spectra from first principles. *Physical Review B - Condensed Matter and Materials Physics*, 62(8):4927 – 4944, 2000.

[37] Stefan Grimme, Jens Antony, Stephan Ehrlich, and Helge Krieg. A consistent and accurate ab initio parametrization of density functional dispersion correction DFT-D for the 94 elements H-Pu. *Journal of Chemical Physics*, 132(15), 2010.

[38] Shuichi Nosé. A unified formulation of the constant temperature molecular dynamics methods. *The Journal of Chemical Physics*, 81(1):511–519, 07 1984.

[39] William G. Hoover. Canonical dynamics: Equilibrium phase-space distributions. *Phys. Rev. A*, 31:1695–1697, Mar 1985.

[40] Atsushi Togo and Isao Tanaka. First principles phonon calculations in materials science. *Scripta Materialia*, 108:1–5, 2015.

[41] Stefano Baroni, Stefano De Gironcoli, Andrea Dal Corso, and Paolo Giannozzi. Phonons and related crystal properties from density-functional perturbation theory. *Reviews of Modern Physics*, 73(2):515 – 562, 2001. Cited by: 8085; All Open Access, Green Open Access.

[42] Duy Khanh Nguyen, Nguyen Thanh Tien, J. Guerrero-Sanchez, and D. M. Hoat. A systematic investigation of chromium and vanadium impurities in a janus Ga_2SO monolayer towards spintronic applications. *Phys. Chem. Chem. Phys.*, 26:18426–18434, 2024.

[43] Ahmad I. Amin B. Khan, F. et al. Density functional theory-based strain engineering of electronic optical and thermoelectric properties of A_2OX (A=Ga,in and X=S,Se) monolayers. *Appl. Phys. A*, 130:456, 2024.

[44] Holleitner A.W. Kastl C. Ozdemir, I. et al. Thickness and defect dependent electronic, optical and thermoelectric features of WTe_2. *Sci Rep*, 12:12756, 2022.

[45] B. Rahman Rano, Ishtiaque M. Syed, and S.H. Naqib. Elastic, electronic, bonding, and optical properties of WTe2 Weyl semimetal: A comparative investigation with $MoTe_2$ from first principles. *Results in Physics*, 19:103639, 2020.

[46] Jinghan Wang, Ju Li, Sidney Yip, Dieter Wolf, and Simon Phillpot. Unifying two criteria of Born: Elastic instability and melting of homogeneous crystals. *Physica A: Statistical Mechanics and its Applications*, 240(1):396–403, 1997. Proceedings of the Euroconference on the microscopic approach to complexity in non-equilibrium molecular simulations.

[47] Zhen Zhang and John T. Jr. Yates. Band bending in semiconductors: Chemical and physical consequences at surfaces and interfaces. *Chemical Reviews*, 112(10):5520–5551, 2012. PMID: 22783915.

[48] Quanlong Xu, Liuyang Zhang, Jiaguo Yu, Swelm Wageh, Ahmed A. Al-Ghamdi, and Mietek Jaroniec. Direct Z-scheme photocatalysts: Principles, synthesis, and applications. *Materials Today*, 21(10):1042–1063, 2018.

[49] Xiao-Ting Li, Chuan-Lu Yang, Wen-Kai Zhao, and Yu-Liang Liu. Photocatalytic Z-scheme overall water splitting for hydrogen generation with Sc_2CCl_2/ML (ML = $MoTe_2$, Hf_2CO_2) heterostructures. *International Journal of Hydrogen Energy*, 59:214–223, 2024.

[50] Wenjun Chen, Jingkai Yang, Yan Zhu, Yinhe Zhang, Yuxuan Zhao, Yintang Wen, and Bo Liang. A direct Z-scheme Janus-MoSSe/$BiVO_4$ heterostructure for photocatalytic water splitting: a first-principles study. *Journal of Physics D: Applied Physics*, 55(30):305501, may 2022.

[51] Hui Wang, Wenxiu Liu, Xin He, Peng Zhang, Xiaodong Zhang, and Yi Xie. An Excitonic Perspective on Low-Dimensional Semiconductors for Photocatalysis. *Journal of the American Chemical Society*, 142(33):14007–14022, 2020. PMID: 32702981.

[52] Cen-Feng Fu, Jiuyu Sun, Qiquan Luo, Xingxing Li, Wei Hu, and Jinlong Yang. Intrinsic Electric Fields in Two-dimensional Materials Boost the Solar-to-Hydrogen Efficiency for Photocatalytic Water Splitting. *Nano Letters*, 18(10):6312–6317, 2018.

[53] Yingcai Fan, Junru Wang, and Mingwen Zhao. Spontaneous full photocatalytic water splitting on 2D $MoSe_2$/$SnSe_2$ and WSe_2/$SnSe_2$ vdW heterostructures. *Nanoscale*, 11:14836–14843, 2019.

[54] Pengzuo Chen, Tianpei Zhou, Mengxing Zhang, Yun Tong, Chengan Zhong, Nan Zhang, Lidong Zhang, Changzheng Wu, and Yi Xie. 3D Nitrogen-Anion-Decorated Nickel Sulfides for Highly Efficient Overall Water Splitting. *Advanced Materials*, 29(30):1701584, 2017.

[55] Ravi K. Biroju, Deya Das, Rahul Sharma, Shubhadeep Pal, Larionette P. L. Mawlong, Kapil Bhorkar, P. K. Giri, Abhishek K. Singh, and Tharangattu N. Narayanan. Hydrogen Evolution Reaction Activity of Graphene–MoS_2 van der Waals Heterostructures. *ACS Energy Letters*, 2(6):1355–1361, 2017.

Journal Pre-proof

Journal Pre-proof

[56] Ziyi Xiao, Wei Zhou, Baopeng Yang, Chengan Liao, Qing Kang, Gen Chen, Min Liu, Xiaohe Liu, Renzhi Ma, and Ning Zhang. Tuned d-band states over lanthanum doped nickel oxide for efficient oxygen evolution reaction. *Nano Materials Science*, 5(2):228–236, 2023. (Photo) Electrochemical Materials and Devices.

[57] Jie Meng, Jiajun Wang, Jianing Wang, Qunxiang Li, and Jinlong Yang. C_7N_6/Sc_2CCl_2 Weak van der Waals Heterostructure: A Promising Visible-Light-Driven Z-Scheme Water Splitting Photocatalyst with Interface Ultrafast Carrier Recombination. *The Journal of Physical Chemistry Letters*, 13(6):1473–1479, 2022. PMID: 35129359.

Journal Pre-proof

Journal Pre-proof

Strain-Induced 11.46% Solar-to-Hydrogen Efficiency in Ga_2SO/WTe_2 Z-scheme Heterostructure

Mengran Qin, Xiangjie Chen, Jifan Wan, Yao He, Kai Xiong

July 18, 2025

Data Availability Statement

The data that support the findings of this study are available from the corresponding author upon reasonable request.

Journal Pre-proof

Journal Pre-proof

Supplementary Material Strain-Induced 11.46% Solar-to-Hydrogen Efficiency in Ga_2SO/WTe_2 Z-scheme Heterostructure

Mengran Qin[1], Xiangjie Chen[1], Jifan Wan[1], Yao He*[1], and Kai Xiong[2]

[1]Department of Physics, Yunnan University
[2]Materials Genome Institute, School of Materials and Energy, Yunnan University

July 18, 2025

CRediT Author Statement

Mengran Qin: Conceptualization, Methodology, Writing - Original Draft. **Xiangjie Chen**: Validation, Formal analysis, Data Curation. **Jifan Wan**: Investigation, Visualization. **Yao He**: Supervision, Project administration, Funding acquisition, Writing - Review & Editing. **Kai Xiong**: Software, Resources, Supervision.

*Corresponding author

Journal Pre-proof

Journal Pre-proof

Declaration of interests

☒ The authors declare that they have no known competing financial interests or personal relationships that could have appeared to influence the work reported in this paper.

☐ The authors declare the following financial interests/personal relationships which may be considered as potential competing interests:

Journal Pre-proof